ACS OMEGA

http://pubs.acs.org/journal/acsodf

Article

Facile Preparation of Fluorescent Carbon Dots from Glutathione and L-Tryptophan for Sensitive and Selective Off/On Detection of Fe^{3+} Ions in Serum and Their Bioimaging Application

Bowen Zhang, Wei Liu, Xiangrong Wu, Jinhua Zhu,* Weiping Hu, Abdelhadi El Jaouhari, and Xiuhua Liu*

Cite This: *ACS Omega* 2022, 7, 7853−7864

Read Online

ACCESS | Metrics & More | Article Recommendations

ABSTRACT: In the past decade, carbon dots (CDs) have attracted considerable attention due to their excellent properties such as low toxicity, good biocompatibility, good fluorescence imaging, etc. Here, glutathione and L-tryptophan were used as carbon sources to hydrothermally synthesize CDs for sensitive and selective off/on detection of Fe^{3+} ions. The CDs are spherical nanoparticles with an average particle size of 3.8 nm and the presence of organic groups such as hydroxyl, carboxyl, sulfhydryl, and amino groups on their surface. The experiment results display that Fe^{3+} ions can be selectively and sensitively detected by quenching the fluorescence of CDs. Moreover, the fluorescence of the CDs+Fe^{3+} system can be restored after adding ascorbic acid. Thus, an off/on fluorescent probe for the determination of Fe^{3+} can be formed using the as-synthesized CDs solution. The CDs show a good linear range of 0−13.89 mM and a 0.0331 μM limit of detection for Fe^{3+}, and the most probable mechanism concluded from ultraviolet−visible spectroscopy, electrospray ionization−mass spectrometry, and fluorescence spectrophotometry is a mixed static and dynamic quenching. Furthermore, the cytotoxicity experiment results show that CDs have low toxicity and can be used for intracellular imaging.

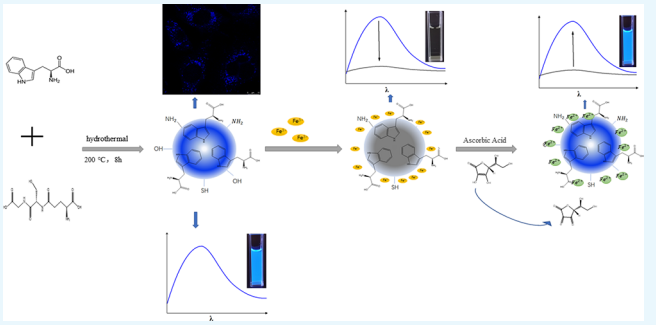

1. INTRODUCTION

Iron is an essential element for all living organisms including humans, and it is also very important in diverse metabolic processes, such as its combination with hemoglobin to participate in oxygen transfer,[1] electron transport,[2] and as a catalyst for DNA synthesis.[3] However, a high iron concentration can cause serious damage to several vital organs and tissues (due to the formation of free radicals). Therefore, it is significant to develop a high-performance system for the detection of iron and its ions in different media.[4] Various analytical techniques such as atomic absorption spectroscopy,[5] electrochemical analysis methods,[6] inductively coupled plasma atomic emission,[7] atomic fluorescence spectrometry,[8] UV−vis spectroscopy,[9] high-pressure ion chromatography,[10] and X-ray spectrometry[11] have been applied for the detection of iron ions. Nonetheless, most of these techniques have certain disadvantages, such as expensive equipment needed, vulnerability to common interference, long time consumption, the use of toxic organic reagents, and low sensitivity, which limit their practical application.[12,13] However, compared with the above mentioned techniques, fluorescence spectrometry has been considered to be a rapid, simple, sensitive, and selective technique for metal ion detection.[14] On the other hand, carbon dots (CDs) are dispersed spherical carbon particles with a dimension of less than 10 nm and possess excellent fluorescence, photochemical, and chemiluminescent properties.[15] Carbon nanodots,[16] graphene quantum dots,[15] and polymer dots[17] are all CDs. Additionally, CDs also present several unique properties, such as low preparation[18] cost, environmental friendliness, outstanding photobleaching resistance,[19] adjustable fluorescence wavelengths,[20] good dispersion, large-scale production, good biocompatibility, and low toxicity. Therefore, they have been widely used in biosensors,[21] bioimaging,[22] drug loading,[23] improved microluminescent diodes, tumor-targeted therapy,[24] catalysis, secondary batteries, and supercapacitors,[25] and agriculture.[26]

CDs are usually composed of surface groups and carbon cores.[27] The organic groups on their surface include −OH,

Received: November 30, 2021
Accepted: February 14, 2022
Published: February 22, 2022

https://doi.org/10.1021/acsomega.1c06757
ACS Omega 2022, 7, 7853−7864

−COOH, NH_2, −SH, etc.,[28] which can be greatly changed and modified by varying the precursors and the doping agents. The diversity of surface groups makes it possible for CDs to become fluorescent probes for the detection of many metal ions.[29] For instance, Liu et al. reported extraordinarily sensitive CDs synthesized by a hydrothermal method for the detection of Cu^{2+}, with a wide linear range (0−50 μM) and a low detection limit (1 nM).[30] Chen et al. proposed the synthesis of CDs with high sensitivity toward Fe^{3+} by a microwave-assisted method with glutamine and acetamide as raw materials. The as-prepared CDs show a good linear range of 8−80 μM, and the limit of detection (LOD) is 3.8 μM for Fe^{3+}.[31] Li et al. synthesized carbazide-based CDs using citric acid as a precursor, and the prepared fluorescent sensor has a good linear range for the detection of Fe^{3+} (0.4−100 μM), Pb^{2+} (100−600 μM), and Hg^{2+} (20−200 μM).[32]

Tryptophan is an important nutrient in the body. As an essential amino acid, it can participate in the synthesis of proteins, and it is also an important prerequisite for auxin biosynthesis in some plants. Tryptophan is very important in organism biosynthesis. Because there are carboxyl, amino, and indole groups on its surface, it can be modified into different structural units. Therefore, tryptophan is a kind of carbon-containing material with good biological properties, low price, and easy availability. Many studies have shown that the doping of heteroatoms such as nitrogen, sulfur, phosphorus, boron, and other elements can significantly improve the optical properties of CDs.[27−29] Glutathione is a tripeptide compound containing amide bonds and sulfhydryl and carboxyl groups, so the properties of CDs can be further optimized and their application range can be broadened by doping sulfur and other heteroatoms with glutathione.

Therefore, based on the above advantages, in the present work, nitrogen- and sulfur-doped CDs were synthesized with a hydrothermal method using L-tryptophan and glutathione as raw materials. The prepared CDs emit strong blue fluorescent light near to 440 nm. The structure of CDs was characterized by X-ray photoelectron spectroscopy (XPS), Fourier transform infrared spectroscopy (FTIR), powder X-ray diffraction (PXRD), and UV−vis spectroscopy, and their fluorescence properties were investigated in the presence of Fe^{3+}. It was found that the CDs demonstrated a good linearity to Fe^{3+} in the concentration range of 0−13.89 mM, and the LOD was 0.0331 μM. The quenched fluorescence of CDs by Fe^{3+} can be restored by adding ascorbic acid (AA), forming a fluorescence "off/on" system to detect Fe^{3+}. The cytotoxicity test and intracellular imaging results proved that CDs have a promising application prospect in biological fields.

2. MATERIALS AND METHODS

2.1. Materials and Instruments. All used chemicals were of analytical grade. L-Tryptophan, glutathione, ascorbic acid, and ferric chloride were obtained from Shanghai Aladdin Biochemical Technology Co., Ltd. (Shanghai, China). Hydrochloric acid (HCl), sodium hydroxide, dopamine hydrochloride, and potassium chloride were purchased from Tianjin Deen Chemical Reagent Co., Ltd. (Tianjin, China). The serum was from a local hospital. Ultrapure water was used throughout.

The chemical composition of the CDs was analyzed with an AXIS ULTRA X-ray photoelectron spectrometer (XPS) (Shimadzu/Kratos, Japan). The fluorescence measurements were carried out on an FLS920 fluorescence spectrophotometer (Edinburgh, Britain). The Fourier transform infrared (FTIR) spectrum of the CDs was recorded using a Nicolet 170sx (Brooke, Germany). Powder X-ray diffraction (PXRD) diagrams were acquired with a Philips X-ray diffractometer with Cu Kα radiation field emission (λ = 1.54178 Å, continuous, 30 kV, 30 mA). Transmission electron microscopy (TEM) and high-resolution transmission electron microscopy (HRTEM) pictures were taken with a JEOL JEM-2010 microscope with an accelerating voltage of 200 kV. Mass spectrometry (MS) was performed using a Bruker Amazon SL instrument. Ultraviolet−visible (UV−vis) absorption spectra were measured by a TU-1900 spectrophotometer (Beijing, China). An inductively coupled plasma atomic emission (ICP-AES) spectrometer (Varian, USA) was used to test iron ions.

2.2. Synthesis of Carbon Dots (CDs). For CDs synthesis, glutathione (0.3010 g) and L-tryptophan (0.1022 g) were dissolved in 10 mL of ultrapure water. The mixed solution was then transferred to a high-pressure kettle (30 mL) lined with Teflon and heated at 200 °C for a certain time; then, the reactor was automatically cooled to room temperature. The solution was centrifuged at 16000 r/min for 5 min, the precipitate was washed with ultrapure water three times, and the washing solution was combined with the supernatant to obtain black solid CDs by freeze-drying.[33]

2.3. Determination of Fe^{3+} Ions and AA. The fluorescence emission spectra were recorded at 364 nm. The slit widths of emission and excitation were both 1 nm. The fluorescence analysis of Fe^{3+} and AA was carried out according to the following procedure. First, 30 μL of CDs solution was diluted to 3 mL with ultrapure water to give a concentration of 1 μg/mL; then, different volumes of Fe^{3+} ions were added to investigate the fluorescence variation of the system. Then, different volumes of AA solution (0.1 M) were injected into the system, and the fluorescence emission spectra were recorded after incubating for 5 min. Thus, Fe^{3+} ions and AA were determined by the fluorescence variation of the system.

2.4. Serum Sample Analysis. To validate the practical application of CDs, Fe^{3+} in serum was tested. Fresh blood was obtained from local hospitals and pretreated according to the methods reported in the literature.[34] The procedure was as follows: 5 mL of nitric acid (8 M) was added into 1.0 mL of a serum sample and kept for 0.5 h. Then, it was evaporated and heated until carbonized. After that, it was ashed at 500 °C for 1 h and cooled to room temperature. Then, the ash was soaked into 1 mL of nitric acid (8 M) and evaporated again. Then, it was ashed again at 500 °C for 0.5 h. After cooling, the residue was dissolved four times with 1 mL of nitric acid (3 M), and the solution was transferred into a volumetric flask and diluted with water to 10 mL. The solution was reserved as a sample for the following test.

2.5. Cytotoxicity Test and Cell Imaging. The cytotoxicity of CDs in vitro was investigated by standard MTT assay. The 3T3-L1 cells were cultured in a 96-well plate with a density of 5000 cells/mL at 37 °C for 24 h. Then, the CDs with different concentrations (0, 100, 200, and 400 μg/mL) were added to each well and incubated at 37 °C under an atmosphere humidified with 5% CO_2 for another 24 h. Subsequently, 10 mL of MTT (5 mg/mL) was added to each well. After incubation at 37 °C for another 4 h, the medium was removed, and 100 μL of dimethyl sulfoxide (DMSO) was added into each well and shaken for 2 min. After further incubation for 3 h, the absorbance was measured at 570 nm using a microplate reader (CLARIOstar, BMG Labtech, Offenburg, Germany).

For cell imaging, the 3T3-L1 cells were first cultured overnight at 37 °C in a DMEM medium supplemented with

https://doi.org/10.1021/acsomega.1c06757
ACS Omega 2022, 7, 7853−7864

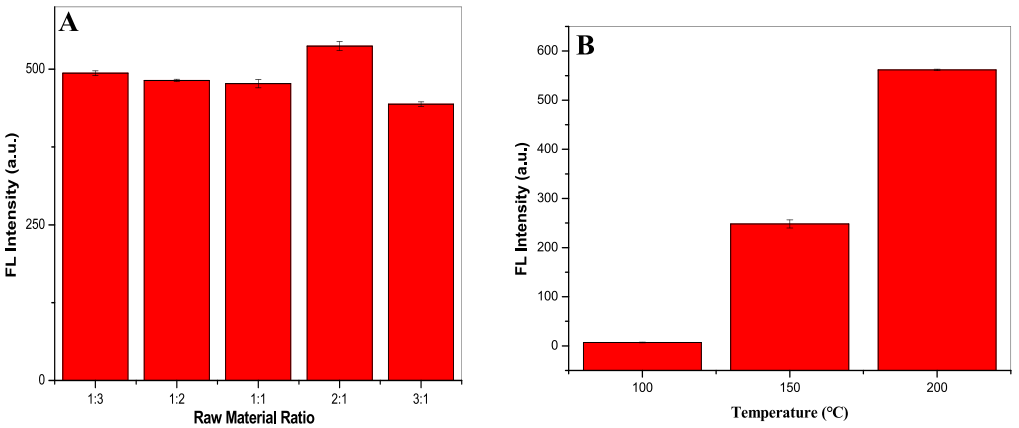

Figure 1. Effects of (A) molar ratios of glutathione to L-tryptophan and (B) reaction temperature on the fluorescence intensity (λ_{em} = 441 nm) of CDs.

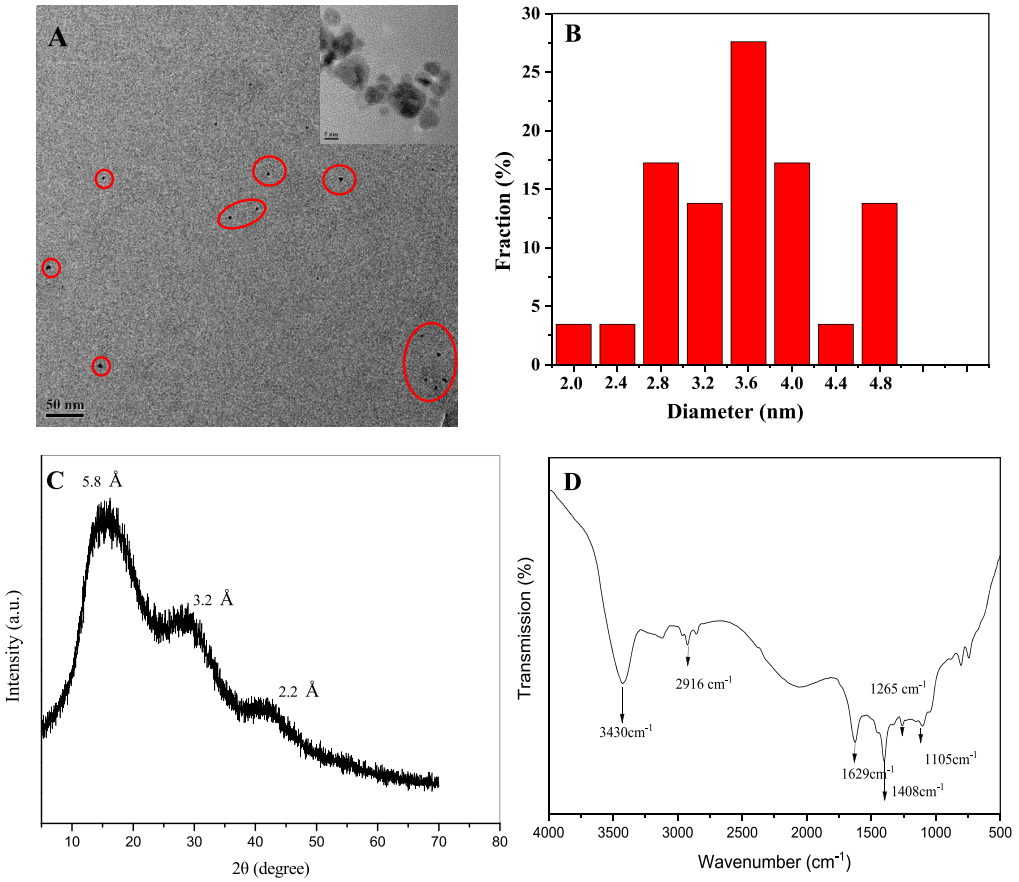

Figure 2. TEM/HRTEM image (A/inset), particle size distribution (B), XRD pattern (C), and FT-IR spectrum (D) of CDs.

10% FBS and 5% CO_2 and then incubated with 0, 200, 400, and 800 μg/mL CDs for 24 h. After that, the supernatant was discarded, and cells were washed three times with PBS buffer to eliminate free CDs. Finally, cell imaging of the treated cells was conducted on a LEICA TCS SPB+ STED confocal microscope (Leica Instruments, Germany).

3. RESULTS AND DISCUSSION

3.1. Characterization of CDs. The ratio of glutathione to L-tryptophan affected the fluorescence of CDs. Thus, the effects of different molar ratios of glutathione to L-tryptophan (1:3, 1:2, 1:1, 2:1, and 3:1) on the fluorescence of CDs were investigated. The results showed that the ratio of glutathione to L-tryptophan had no obvious effect on the fluorescence intensity of CDs. When the ratio of glutathione to L-tryptophan was 2:1, the fluorescence intensity was relatively higher (Figure 1A). Therefore, 2:1 was chosen as the optimum molar ratio. In addition, the influence of hydrothermal synthesis temperature (100, 150, and 200 °C) on the fluorescence intensity of CDs was also studied. The results demonstrated that the fluorescence intensity of the product increased with the increase in heating temperature, indicating that the higher the temperature, the more thorough the carbonization of raw materials, which was beneficial to the formation of carbon dots (Figure 1B). Therefore, the optimal synthesis temperature was selected to be 200 °C. The reaction time (4, 6, 8, 10, and 12 h) was also

https://doi.org/10.1021/acsomega.1c06757
ACS Omega 2022, 7, 7853−7864

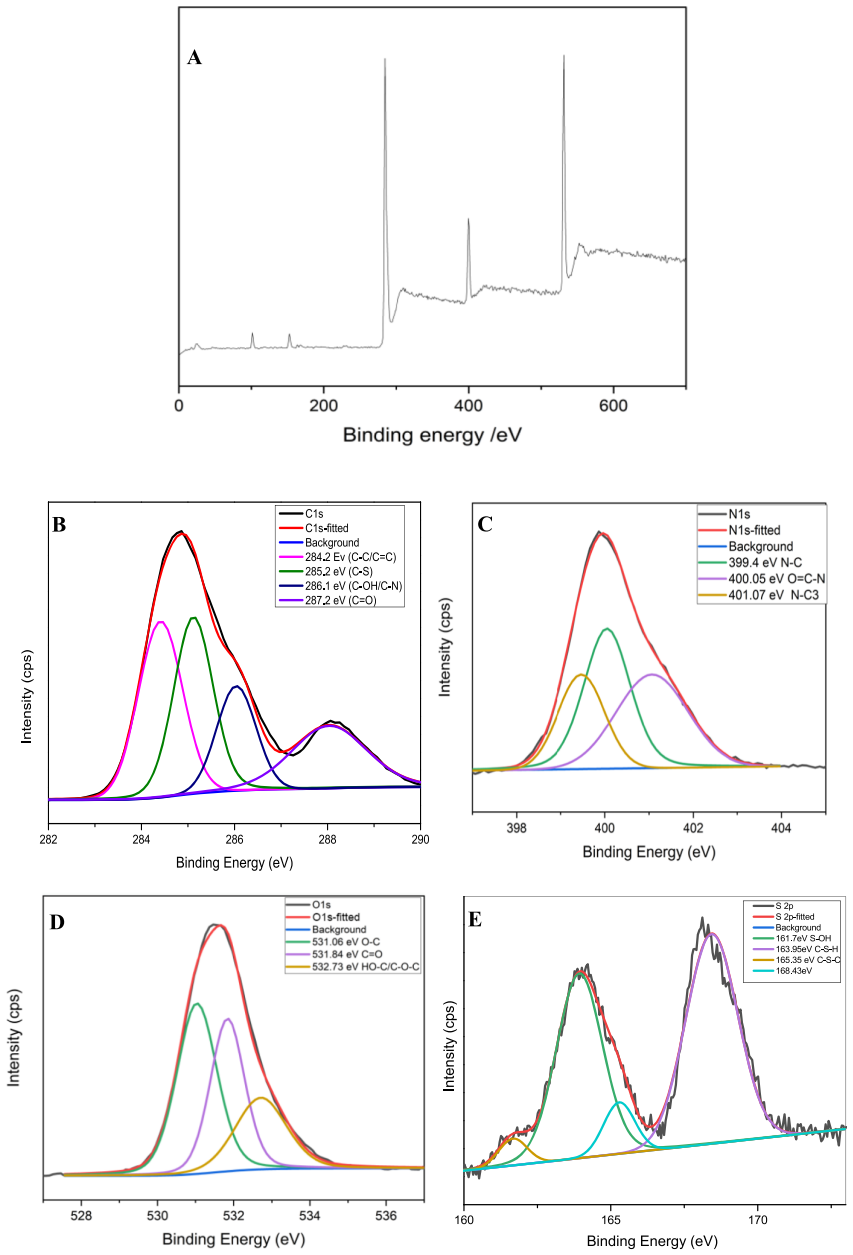

Figure 3. XPS spectra of CDs (A). High-resolution spectra of C 1s, N 1s, O 1s, and S 2p (B–E).

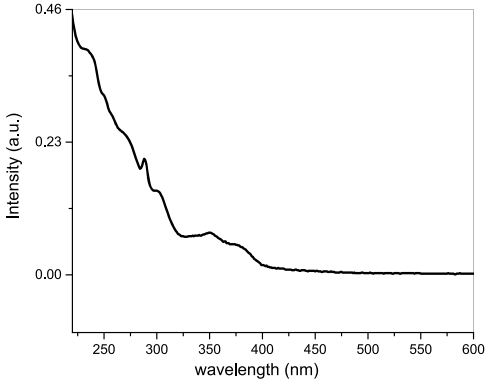

Figure 4. UV–vis absorption spectrum of CDs.

optimized. The fluorescence intensity of carbon dots increased during the reaction time increasing from 4 to 8 h, indicating that increasing the reaction time can make the reaction of glutathione and L-tryptophan with water more sufficient. However, the fluorescence intensity remained almost the same after 8 h. Considering energy consumption, the optimal reaction time was finally selected to be 8 h. Under the optimum synthetic conditions (glutathione to L-tryptophan was 2:1, synthesis temperature was 200 °C, and reaction time was 8 h), CDs were synthesized and characterized.

The morphology of the CDs was characterized by TEM. Figure 2A shows that the CDs are well-dispersed spherical nanoparticles with an average particle size of about 3.8 nm (Figure 2B). The XRD graph of CDs (Figure 2C) shows three diffraction peaks, which are similar to typical diffraction peaks of graphite oxide. For specification, the (001) plane is located at 15.5° (d_{001} = 0.58 nm) near the diffraction peak 2θ = 10.61°, and this difference is probably due to the increase in the sp^3 layer spacing[35] of the synthesized CDs. The second XRD peak appears at 27° (d_{002} = 0.32 nm), which corresponds to the

https://doi.org/10.1021/acsomega.1c06757
ACS Omega 2022, 7, 7853−7864

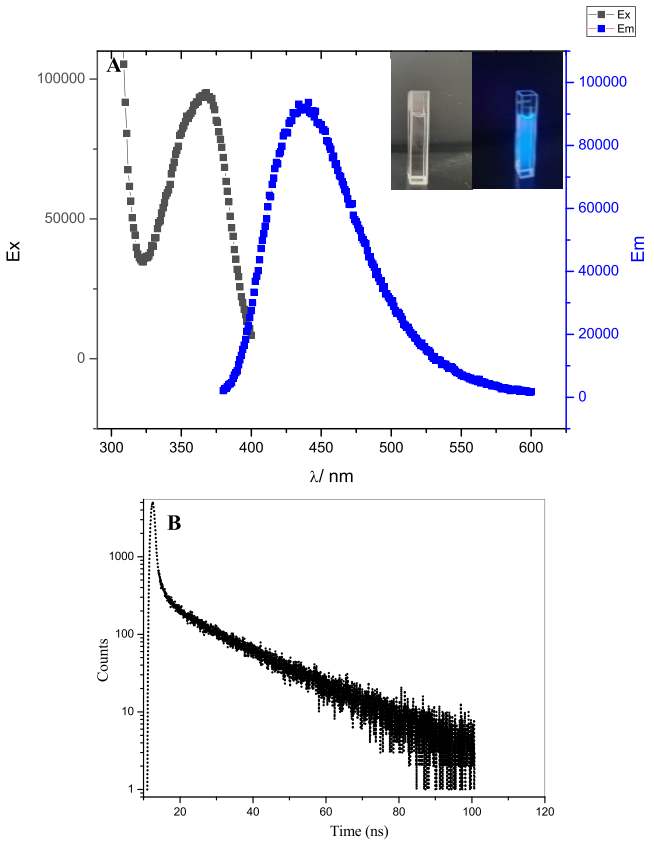

Figure 5. (A) Fluorescence spectra of CDs, the insets are the photographs of CDs under natural light (left) and UV light at 365 nm (right). (B) Fluorescence lifetime spectra of CDs.

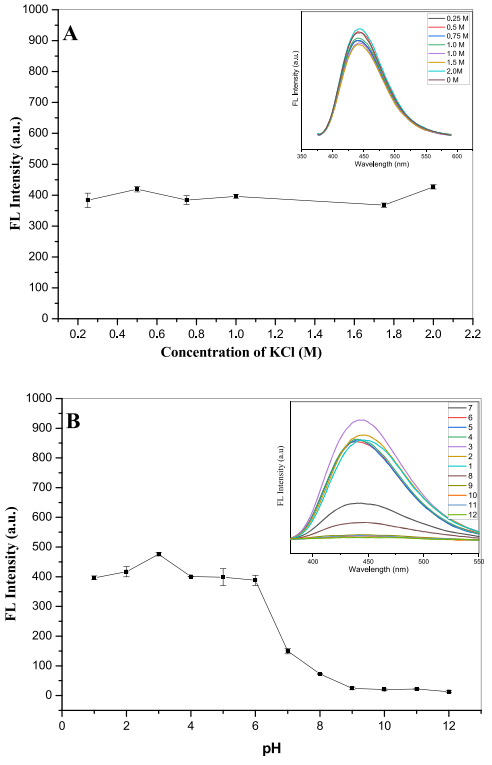

Figure 6. Influence of ionic concentration (KCl) (A) and pH (B) on the fluorescence intensity of CDs.

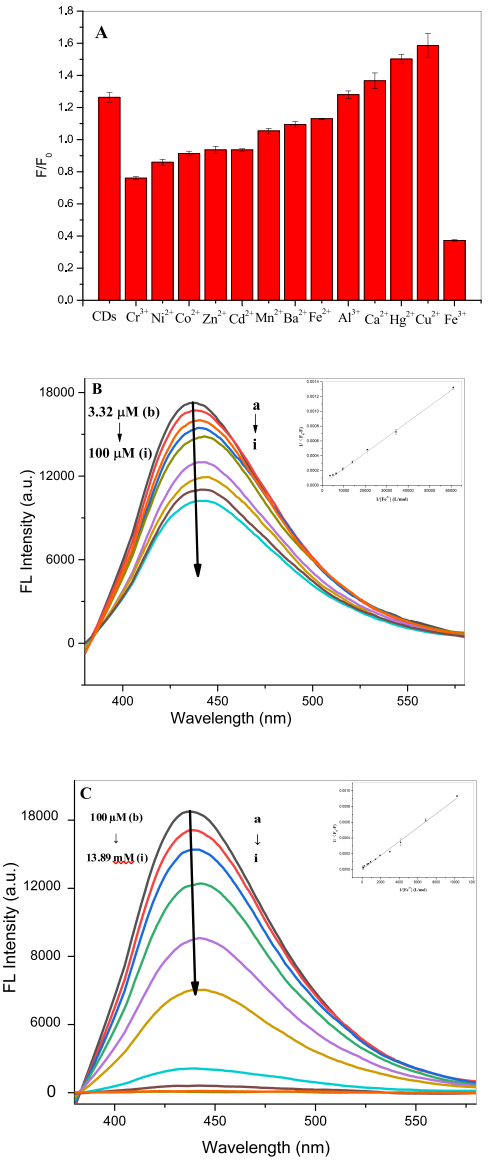

Figure 7. (A) Influence of different metal ions (3.23 mM) on the fluorescence intensity of CDs (λ_{em} = 441 nm, λ_{ex} = 364 nm). (B,C) Fluorescence emission spectra of CDs solution (a, 0.001 mg/mL) at various concentrations of Fe^{3+} (b→i), λ_{ex} = 364 nm. The insets are the linear relationship between $1/(F_0 - F)$ and $1/[Fe^{3+}]$.

graphite-like stacking of conjugated aromatic structures.[36] While the third diffraction peak of CDs is located at $2\theta = 41°$ (d_{010} = 0.225 nm), which is similar to the hexagonal structure of graphite, indicating that the CDs have poor crystallinity and have multilayered structures with nonhomogeneous phases.[37] FT-IR spectroscopy was performed to analyze the functional groups of CDs (Figure 2D). As it is shown, the characteristic absorption bands located at 3430 cm^{-1} correspond to the O−H/N−H stretching vibrations, and the symmetric and asymmetric stretching vibrations of the C−H absorption bands can be observed at 2916 and 1408 cm^{-1}, respectively. Meanwhile, the absorption bands located at 1629 and 1105 cm^{-1} are assigned to −C═ONH and −C−O stretching vibrations, respectively.[21,23,38] The XPS spectrum of CDs consists of four peaks, which corresponds to S 2p (164 eV), C 1s (286 eV), N 1s (401 eV), and O1s (533 eV), as shown in

https://doi.org/10.1021/acsomega.1c06757
ACS Omega 2022, 7, 7853−7864

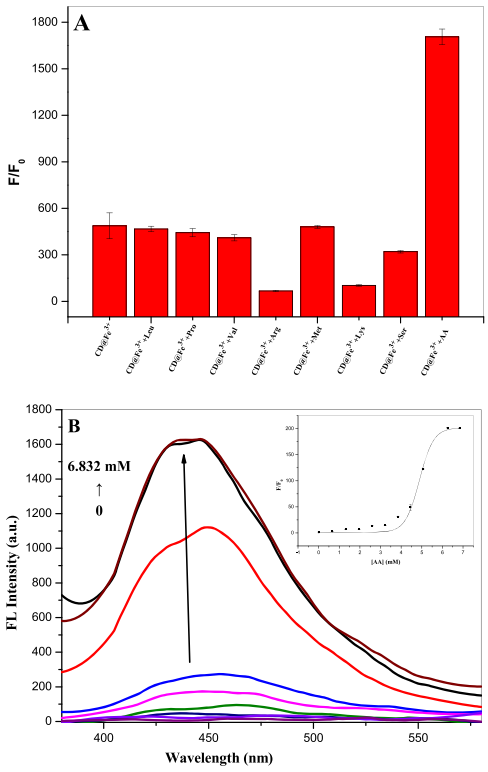

Figure 8. (A) Fluorescence of CDs+Fe^{3+} with 2.94 mM of different biomolecules (λ_{em} = 441 nm, λ_{ex} = 364 nm). (B) Fluorescence emission spectra of CDs solution (0.001 mg/mL) with 11.77 mM Fe^{3+} at different concentrations of AA, λ_{ex} = 364 nm. The inset is the relationship between F_0/F and the concentrations of AA.

Figure 3A. The high-resolution spectrum of C 1s can be deconvoluted into four peaks, which are located at 284.2, 285.2, 286.1, and 287.2 eV, which are attributed to C═C, C−S, C−O−H/C−N, and C═O, respectively (Figure 3B).[39,40] The N 1s spectrum confirmed the presence of NH_2 at 399.4 eV, O═C−N at 400.05 eV,[41] and N−C_3 at 401.07 eV[42] (Figure 3C). The deconvoluted O 1s spectrum has three peaks, which are located around 531.06, 531.84, and 532.73 eV. The peak around 531.06 eV corresponds to O−C, the O═C peak is located at 531.84 eV, while the peak around 532.73 eV can be assigned to O in C−O−C and C−OH bonds[41,43] (Figure 3D). Finally, Figure 3E shows the spectrum of S 2p, which can be deconvoluted into four peaks located at 168.43, 165.35, 163.95, and 161.7 eV, corresponding to sulfate oxide, C−S−C, C−S−H, and thiol groups, respectively.[44]

The above results demonstrate that there are abundant organic groups including −OH, −COOH, $-NH_2$, −SH, etc. on the surface of the synthesized CDs, which provides the possibility for its subsequent application.

The fluorescence and UV−vis absorption spectra were investigated for the synthesized CDs. The UV−vis absorption spectrum of CDs is illustrated in Figure 4. As can be seen, the absorption peak at 237 nm is attributed to the $\pi-\pi^*$ transition of the aromatic sp^2 domain, while the peaks at 271 and 349 nm correspond to the p−p*of C−C and the n−p*of C−O absorption, respectively. The absorption peak at 300 nm is related to the $\pi-\pi^*$ and n−π^* transitions of C═O. For the fluorescence spectrum (Figure 5A), the optimum excitation and emission wavelengths of CDs are 364 and 441 nm, respectively. The aqueous solution of CDs shows blue fluorescence under irradiation of a 360 nm UV lamp; however, the transparent solution can be seen under sunlight. Its absolute fluorescence quantum yield is 35.54% measured by an absolute PLQY measurement system (FluoroLog-3) with an integrating sphere. The fluorescence lifetime can be defined as the time elapsed between the activation of the fluorophore and the emission of photons by the fluorophore.[45] By measuring the fluorescence lifetime, we can get information about its molecular structure and kinetics. The average fluorescence lifetime of CDs was investigated to be 18.2 ns (Figure 5B). The relatively long fluorescence lifetime of the CDs prompts us to further study their application in living organism imaging.

3.2. Stability Research of CDs. The fluorescence stability of CDs solutions with different concentrations of KCl (0, 0.5, 0.75, 1.5, and 2 mol/L) and different pH values (1−13) was investigated. From the results of Figure 6A, it can be concluded that the spectral characteristics and fluorescence intensity of CDs solution are almost unchanged under the effect of different KCl concentrations, indicating that CDs can be applied to salt-rich solutions including body fluids.[46] With regard to the influence of pH, CDs solution presents good fluorescence stability in an acidic medium and has an optimum intensity at pH 3. However, the fluorescence intensity decreases with the increase in alkalinity (Figure 6B); especially, the fluorescence intensity decreases dramatically from pH 6 to 12. This behavior can be explained by the protonation and deprotonation of carboxyl and amino cations on the surface of CDs.[29] This may be because the carboxyl, amino, and hydroxyl groups on the surface of CDs are prone to form hydrogen bonds under alkaline conditions, and the aggregation of CDs will quench some fluorescence, resulting in the lower fluorescence intensity. Under acidic conditions, CDs are protonated, so hydroxyl or carboxyl groups are positively charged and CDs are more

Table 1. Comparison of the Performance of CDs for Fe^{3+} Detection with Other Reported CDs Methods

materials used for synthesizing CDs	methods	linear range (μM)	LOD (μM)	reference
rice	fluorescence off/on	0−50	0.078	44
citric acid and phenylalanine	fluorescence quenching	5.0−500	0.720	46
medium−low-temperature coal tar pitch	fluorescence off/on	0−50	0.173	47
pineapple	fluorescence quenching	0.05−500	0.03	48
p-aminosalicylic acid and ethylene glycol dimethacrylate	fluorescence off/on	0.05−10.0	0.0137	49
glutamic acid and ethylenediamine	fluorescence quenching	8−80	3.8	31
citric acid	fluorescence quenching	0.4−100	2.8	32
PEG-diamine and citric acid	fluorescence quenching	0.01−500	0.0025	18
tryptophan and glutathione	fluorescence off/on	0−100 100−1.39 × 10^4	0.0331	present work

https://doi.org/10.1021/acsomega.1c06757
ACS Omega 2022, 7, 7853−7864

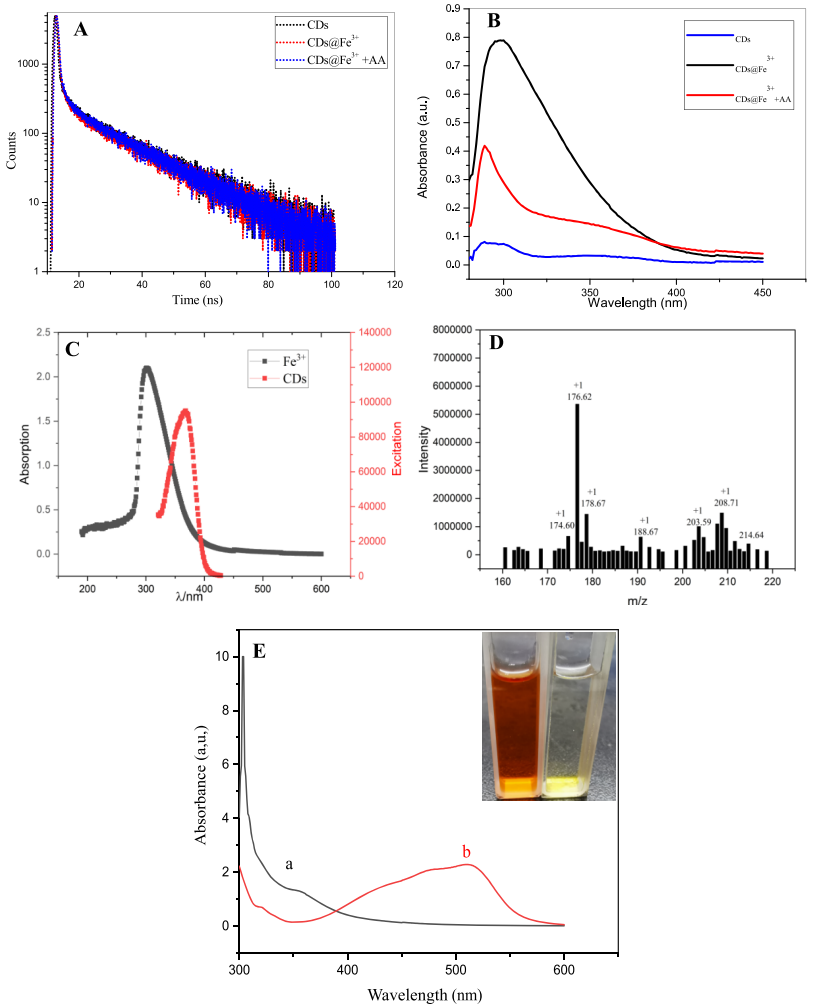

Figure 9. (A) Fluorescence lifetime of CDs in the presence of Fe^{3+} and Fe^{3+}+AA. (B) UV−vis spectra of CDs, CDs+Fe^{3+}, and CDs+Fe^{3+}+AA solutions. (C) UV−vis absorption spectrum of Fe^{3+} and the fluorescence excitation spectrum of CDs. (D) Mass spectrum of CDs+Fe^{3+} solution after addition of AA. (E) UV−vis spectra of CDs+Fe^{3+}+phen solution before (a) and after treatment with AA (b). Inset: photograph of CDs+Fe^{3+}+phen (right) and CDs+Fe^{3+}+phen+AA (left) under visible light.

Table 2. Determination Results of Fe^{3+} in Serum and Recovery Results

sample	detected (μM)	added (μM)	found (μM)	recovery (%)	RSD (%)
serum	28.04 (9.51%)[a]	64.10	90.21	96.88	2.22
		93.72	120.58	98.72	2.41
	26.25 (0.997)[b]	127.4	150.94	96.06	3.89

[a]The data in brackets is the RSD, n = 5. [b]The data was obtained by the ICP-AES method.

dispersed due to electrostatic charge repulsion, resulting in a higher fluorescence intensity. CDs synthesized by different carbon sources and different methods may have different responses to acids and alkalis due to the different functional groups and the number of functional groups on the surface of CDs, resulting in different influences of pH on CDs.

3.3. Off/On Fluorescence Detection of Fe^{3+} Ions. In order to evaluate their potential application in metal ion detection, the selectivity of CDs was investigated. First, the effects of different cations such as Na^+, K^+, Ni^{2+}, Cd^{2+}, Cu^{2+}, Hg^{2+}, Zn^{2+}, Fe^{2+}, Co^{2+}, Mn^{2+}, Fe^{3+}, Cr^{3+}, and Al^{3+} with the same concentration on the fluorescence response of CDs in water were tested. As shown in Figure 7A, certain metal ions such as

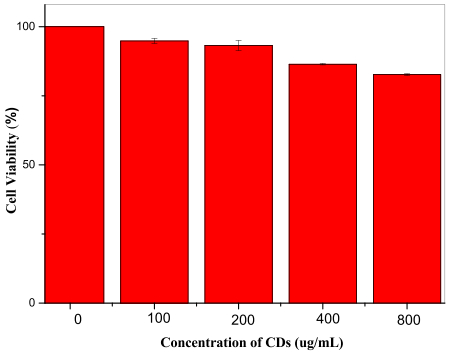

Figure 10. Viability of 3T3-L1 cells after incubation with different concentrations of CDs for 24 h by MTT assay.

Al^{3+}, Fe^{2+}, and Ca^{2+} can slightly enhance the fluorescence intensity of CDs, while Ba^{2+}, Cr^{3+}, Mn^{2+}, and Zn^{2+} have no obvious effect on the fluorescence of CDs. The other ions such as Cd^{2+}, Ni^{2+}, Co^{2+}, Cu^{2+}, and Hg^{2+} can partially quench the fluorescence of CDs; however, the quenching effect is not distinct enough for application, and only Fe^{3+} has a distinct quenching effect on the fluorescence of CDs. Therefore, the CDs can selectively respond to Fe^{3+} in a complex environment.

https://doi.org/10.1021/acsomega.1c06757
ACS Omega 2022, 7, 7853−7864

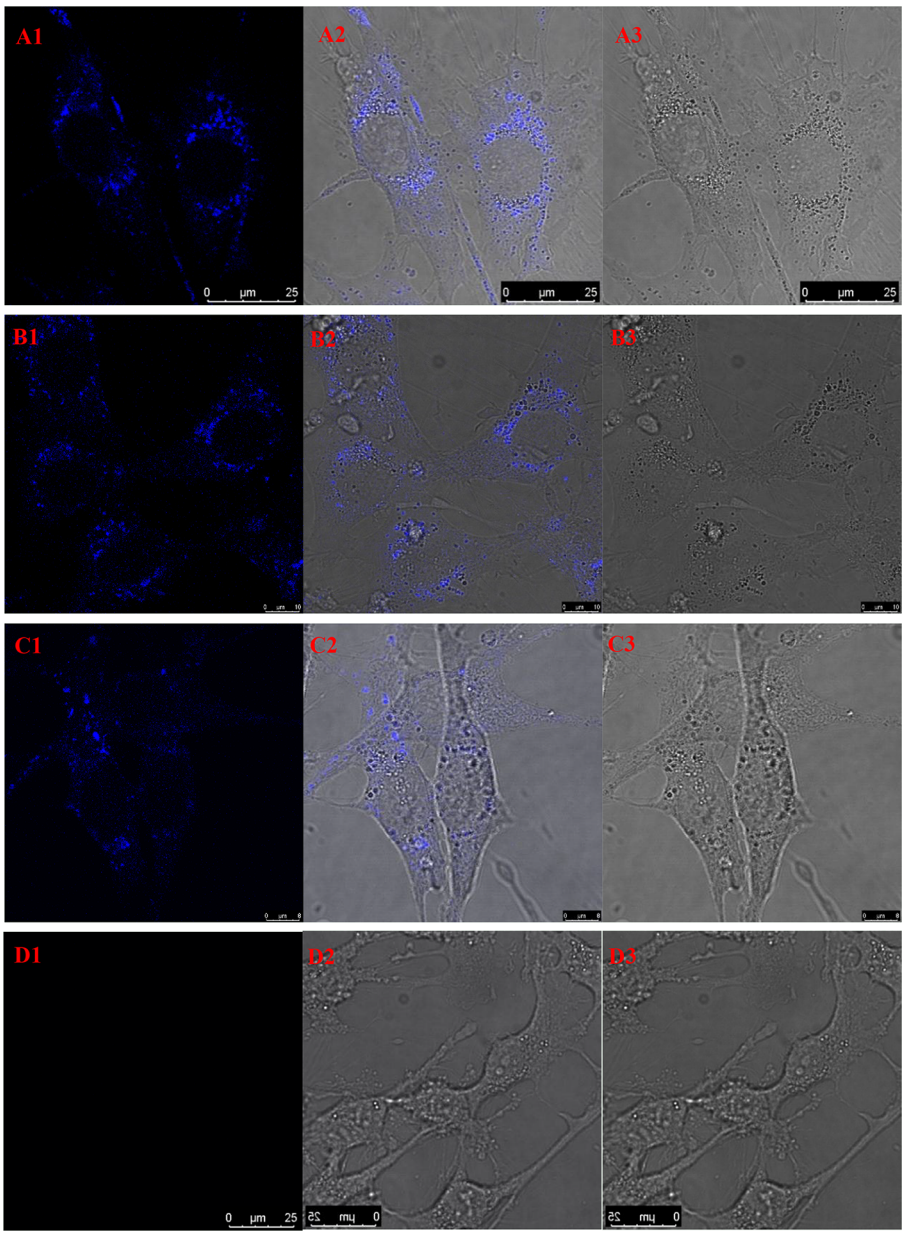

Figure 11. Fluorescence microscopy images of 3T3-L1 cells coincubated with 800 (A), 400 (B), 200 (C), and 0 μg/mL (D) CDs. 1's are obtained under an excitation of 405 nm, 2's are the images under merging, and 3's are the images under a bright field.

As displayed in Figure 7B,C, the fluorescence emission intensity of CDs decreased drastically with the increase in the Fe^{3+} concentration from 3.32 μM to 13.89 mM. Compared with the fluorescence spectrum of the original CDs, the maximum emission wavelength of the system is slightly redshifted after adding different concentrations of Fe^{3+}, indicating that iron(III) ions interact with CDs to form new complexes. Thus, the microenvironment of CDs is changed, and the fluorescence of CDs is quenched. This quenching effect can be approximately quantitatively evaluated by the Benesi−Hildebrand equation:[47]

$$\frac{C^{o}_{CDs}}{F_0 - F} = \frac{1}{K(\varepsilon_{CDs\bullet Fe} - \varepsilon_{CDs})} \times \frac{1}{C^{o}_{Fe^{3+}}} + \frac{1}{(\varepsilon_{CDs\bullet Fe} - \varepsilon_{CDs})} \quad (1)$$

wherein F_0 and F are the fluorescence intensities of CDs before and after Fe^{3+} ion incorporation, C^{o}_{CDs} and $C^{o}_{Fe^{3+}}$ are the initial concentrations of CDs and Fe^{3+}, $\varepsilon_{CDs}$and $\varepsilon_{CDs\bullet Fe}$ are the molar absorption coefficients of CDs and the complex formed by CDs and Fe^{3+}, and K is the equilibrium constant of the composite formed by CDs and Fe^{3+}.

The results show that there is a good linear relationship between $1/(F_0 - F)$ and the reciprocal of Fe^{3+} concentration. In the concentration range of 0−100 μM, the linear regression equation is $y = 5.99 \times 10^{-9}x + 3.17 \times 10^{-4}$ ($r = 0.9939$), and K is calculated from the intercept and the slope to be 5.29×10^{4}. Meanwhile, in the concentration range of 100 μM to 13.89 mM, the linear regression equation is $y = 4.84 \times 10^{-8}x + 3.73 \times 10^{-5}$, the relation coefficient r is 0.9967, and K is calculated to be 7.71×10^{2}. The LOD calculated for Fe^{3+} is 0.0331 μM deriving from $3S/N$ of the blank solution.[48] From the results, it can be seen that Fe^{3+} with a lower concentration can rapidly quench the

https://doi.org/10.1021/acsomega.1c06757
ACS Omega 2022, 7, 7853−7864

fluorescence of CDs by forming the composite. The quantity of CDs is constant (0.001 mg/L); initially, with the addition of Fe^{3+}, they quickly react with the active centers of CDs, and the fluorescence is quenched quickly. As more and more Fe^{3+} is added, the active centers of CDs are gradually consumed, and the reaction speed becomes slower with the slower forming speed of the complex, which can be proven by the lower equilibrium constant. These results further illustrate the sensitivity of this method to detecting Fe^{3+}.

In order to further exploit the feasibility of the above formed CDs+Fe^{3+} for the detection of other compounds of biological interest, CDs+Fe^{3+} was handled with various aqueous solutions such as dopamine, H_2O_2, glycine, and seven other kinds of biomolecules with a concentration of 100 mM (100 μL). Upon mixing for 5 min, only AA was observed to restore the fluorescence of the CDs+Fe^{3+} system accordingly (Figure 8A). The fluorescence of the CDs can be quenched by Fe^{3+}, and the quenched fluorescence can be restored by adding a certain concentration of AA. Thus, an off/on system for the determination of Fe^{3+} and AA was easily established. The fluorescence emission spectra of CDs+Fe^{3+} after adding AA were recorded. When the concentration of AA is lower than 3.23 mM, the fluorescence intensity at 441 nm of CDs+Fe^{3+}+AA gradually increases with increasing of the AA concentration (Figure 8B). The fluorescence intensity of the system increased significantly with a continuous increase in the AA concentration to 6.0 mM and remained unchanged with the further increase in the AA concentration. The fluorescence intensity of the system can be restored to 83.04% of the original fluorescence intensity of CDs without considering the dilution effect. However, for the above interfering ions of Cd^{2+}, Ni^{2+}, Co^{2+}, Cu^{2+}, and Hg^{2+}, which can partially quench the fluorescence of CDs, the quenched fluorescence cannot be restored by adding AA. Therefore, CDs +AA is a fluorescence system with on/off performance and can be used for selective and sensitive determination of Fe^{3+}. Comparing these properties of our proposed CDs system with other methods reported in references (Table 1), it is confirmed that the CDs are more effective in the determination of Fe^{3+} than the previously reported fluorescence method because they provide a wide linear range and a better detection limit (Table 1). Furthermore, the off/on system provides the possibility of the cyclic use of CDs.

3.4. Possible Fluorescence Off/On Mechanism. Generally, there are two types of fluorescence quenching of CDs: static quenching or dynamic quenching.[49] Dynamic quenching reduces the fluorescence intensity due to energy transfer or charge transfer between the fluorescent material and the quenching substance, while static quenching is the combination of the fluorescent material and the quenching substance into a nonluminescent complex.[50] The fluorescence lifetime is often applied to distinguish between dynamic and static annihilation paths. Therefore, fluorescence lifetimes of CDs with and without Fe^{3+} were tested, and the results show that the fluorescence lifetime of CDs has no change before and after the addition of Fe^{3+} (Figure 9A). Even when AA was added to the system to restore the quenched fluorescence, the fluorescence lifetime of this system almost had no change. This phenomenon indicates that the quenching process of fluorescence is static quenching.[51] Furthermore, the changes in the fluorescence intensities were exploited using the Benesi−Hildebrand equation to determine the stoichiometric ratio and the association constant of CDs/Fe^{3+} interaction.[47] It can be seen from Figure 7B,C that $1/(F_0 - F)$ linearly varies with the reciprocal of Fe^{3+} concentration (Benesi−Hildebrand method), affirming that the stoichiometric ratio of CDs:Fe^{3+} is 1:1. Moreover, the equilibrium constant (log K) estimated from the Benesi−Hildebrand equation was 3.72 in the lower concentration and 2.89 in the higher concentration.

In the UV absorption spectrum, the absorption peak at 300 nm increases after the addition of Fe^{3+} (Figure 9B). In addition, it also leads the absorption peak to shift to a longer wavelength, indicating that Fe^{3+} is in coordination with CDs. Therefore, Fe^{3+} and CDs have a synergetic effect. The absorption band of Fe^{3+} is between 300 and 400 nm, while the excitation spectrum of CDs is around 364 nm (Figure 9C), and the absorption band of Fe^{3+} partly overlaps with the excitation spectrum of CDs, revealing that the excitation energy of CDs can be competitively absorbed by Fe^{3+}, resulting in the quenching of the fluorescence of CDs. After the addition of AA, the absorption peak of CDs/Fe^{3+} at 300 nm decreases significantly with a certain blueshift (Figure 9B). This observation indicates that the restoring of fluorescence can be attributed to the redox reaction between Fe^{3+} and AA, where Fe^{3+} is reduced to Fe^{2+}. It is speculated that the enediol groups of AA are oxidized to *ortho*-diones to produce dehydroascorbic acid (DHAA); meanwhile, Fe^{3+} is reduced to Fe^{2+}. To verify such a hypothesis, AA was added into the CDs+Fe^{3+} solution and reacted for 2 min, and the supernatant was analyzed by electrospray ionization−mass spectrometry (ESI−MS). As shown in Figure 9D, the peak at m/z = 176.62^{+1} (calcd. = 175.12) can be assigned to $[DHAA+H]^+$, and the observation proves our previous speculation. In order to validate the formation of Fe^{2+} during the process, the UV absorption spectrum of CDs+Fe^{3+}+1,10-phenanthroline (phen) solution with and without AA was also compared. When phen was added to the CDs+Fe^{3+} solution, a colorless clear solution was observed (Figure 9E). When AA was added to the solution, the color of the solution changed to orange, which can confirm that Fe^{2+} was generated and formed a complex with phen. From the UV absorption spectra, it can be observed that curve b has an obvious absorption band around 510 nm, which can be attributed to the generation of the $[Fe(phen)_3]^{2+}$.[52] These results indicate that the Fe^{3+} is restored to Fe^{2+} when the CDs +Fe^{3+} is treated with AA.

3.5. Real Sample Analysis. We concluded that Fe^{3+} can quench the fluorescence of CDs solution without interference from other ions, and there is a linear relationship between the reciprocal of Fe^{3+} concentration and $1/(F_0 - F)$, indicating that CDs can selectively detect Fe^{3+}. Thus, in order to evaluate their application in biological samples, CDs were applied to detect Fe^{3+} in serum. As shown in Table 2, after disposal, the Fe^{3+} in serum detected is 28.04 μM, which is in accordance with the result determined by the ICP-AES method (26.25 μM). Then, different concentrations of Fe^{3+} were added to the samples, and the fluorescence spectra at an excitation wavelength of 364 nm were recorded to investigate the recovery results. It was calculated that the recoveries of Fe^{3+} were in the range of 96.06−98.72%, and the RSD (n = 4) was below 3.89%. The results demonstrate that the CDs synthesized from glutathione and L-tryptophan can sensitively and selectively detect Fe^{3+} in biological samples.

3.6. Cytotoxicity and Fluorescence Marker Application of CDs. Because CDs have good stability and biocompatibility, human muscle cells 3T3-L1 were used to investigate the cytotoxic effect of CDs using the MTT method. Figure 10 shows the MTT results of cells cultured after 24 h with the increasing concentration of S,N-doped CDs. The cell viability is still above 85% when the concentration of CDs is 400

https://doi.org/10.1021/acsomega.1c06757
ACS Omega 2022, 7, 7853−7864

μg/mL. Further increasing the concentration of CDs to 800 μg/mL, the cell viability can still reach about 80%. In order to further validate the imaging application potential of CDs in biological samples, the bright and fluorescence fields of 3T3-L1 cells in the presence of CDs after 24 h were initially observed by a fluorescence inverted microscope. Figure 11 shows images of bright and fluorescence fields of human muscle cells cultured with CDs. When the excitation wavelength is 405 nm, the cells emit bright blue fluorescence with a low concentration. Laser confocal microscope observation found that S,N-doped CDs could easily pass through the cell membrane and were mainly distributed in the cytoplasm (Figure 11). The prepared CDs have excellent photostability, indicating that the probe has potential applications in the fields of biomedicine and biochemistry.

4. CONCLUSIONS

To sum up, we have successfully prepared novel CDs with a high photoluminescence quantum yield of 35.54% and long lifetimes of 18.2 ns, as well as high stability in high-concentration salt solutions. Moreover, it can be used as a probe for detecting metal ions and biomolecules. The aqueous solution of the CDs exhibits a fluorescence "turn off" phenomenon for Fe^{3+}, which is caused by the formation of compounds between oxygen-containing ions on the surface of CDs. At the same time, AA makes the fluorescence of CDs have the role of "turn on" due to the reaction with Fe^{3+}. This switch for AA and Fe^{3+} has potential applications in disease diagnosis and bioimaging fields.

AUTHOR INFORMATION

Corresponding Authors

Jinhua Zhu − *Henan International Joint Laboratory of Medicinal Plants Utilization, College of Chemistry and Chemical Engineering, Henan University, Kaifeng 475004, China;* orcid.org/0000-0003-2155-2659; Email: zhujinhua0528@163.com

Xiuhua Liu − *Henan International Joint Laboratory of Medicinal Plants Utilization, College of Chemistry and Chemical Engineering, Henan University, Kaifeng 475004, China;* orcid.org/0000-0001-6958-0478; Email: liuxiuhua@henu.edu.cn

Authors

Bowen Zhang − *Henan International Joint Laboratory of Medicinal Plants Utilization, College of Chemistry and Chemical Engineering, Henan University, Kaifeng 475004, China*

Wei Liu − *Henan International Joint Laboratory of Medicinal Plants Utilization, College of Chemistry and Chemical Engineering, Henan University, Kaifeng 475004, China*

Xiangrong Wu − *Henan International Joint Laboratory of Medicinal Plants Utilization, College of Chemistry and Chemical Engineering, Henan University, Kaifeng 475004, China*

Weiping Hu − *Henan International Joint Laboratory of Medicinal Plants Utilization, College of Chemistry and Chemical Engineering, Henan University, Kaifeng 475004, China*

Abdelhadi El Jaouhari − *Henan International Joint Laboratory of Medicinal Plants Utilization, College of Chemistry and Chemical Engineering, Henan University, Kaifeng 475004, China*

Complete contact information is available at: https://pubs.acs.org/10.1021/acsomega.1c06757

Notes

The authors declare no competing financial interest.

ACKNOWLEDGMENTS

This research was funded by the National Science Foundation of China (U2004133) and the Henan University (CJ1205A0240016 and 2019YLZDYJ13).

REFERENCES

(1) Maity, R.; Chakraborty, D.; Nandi, S.; Yadav, A. K.; Mullangi, D.; Vinod, C. P.; Vaidhyanathan, R. Aqueous-Phase Differentiation and Speciation of Fe3+ and Fe2+ Using Water-Stable Photoluminescent Lanthanide-Based Metal-Organic Framework. *ACS Appl. Nano Mater.* **2019**, *2*, 5169−5178.

(2) Dunn, J. O. C.; Mythen, M. G.; Grocott, M. P. Physiology of Oxygen Transport. *BJA Educ.* **2016**, *16*, 341−348.

(3) Goral, V. N.; Zaytseva, N. V.; Baeumner, A. J. Electrochemical Microfluidic Biosensor for the Detection of Nucleic Acid Sequences. *Lab Chip* **2006**, *6*, 414−421.

(4) Li, L.; Wang, C.; Luo, J.; Guo, Q.; Liu, K.; Liu, K.; Zhao, W.; Lin, Y. Fe3+-Functionalized Carbon Quantum Dots: A Facile Preparation Strategy and Detection for Ascorbic Acid in Rat Brain Microdialysates. *Talanta* **2015**, *144*, 1301−1307.

(5) Al-Bagawi, A. H. Analytical and Electroanalytical Techniques in the Determination of (Fe+2) Results from Iron Corrosion: Effect of Omeprazole Drugs as Green Inhibitors. *Green Chem. Lett. Rev.* **2021**, *14*, 71−82.

(6) El Jaouhari, A.; Yan, L.; Zhu, J.; Zhao, D.; Zaved Hossain Khan, M.; Liu, X. Enhanced Molecular Imprinted Electrochemical Sensor Based on Zeolitic Imidazolate Framework/Reduced Graphene Oxide for Highly Recognition of Rutin. *Anal. Chim. Acta* **2020**, *1106*, 103−114.

(7) Jamali, M. R.; Assadi, Y.; Shemirani, F.; Hosseini, M. R. M.; Kozani, R. R.; Masteri-Farahani, M.; Salavati-Niasari, M. Synthesis of Salicylaldehyde-Modified Mesoporous Silica and Its Application as a New Sorbent for Separation, Preconcentration and Determination of Uranium by Inductively Coupled Plasma Atomic Emission Spectrometry. *Anal. Chim. Acta* **2006**, *579*, 68−73.

(8) Mei, Q.; Jiang, C.; Guan, G.; Zhang, K.; Liu, B.; Liu, R.; Zhang, Z. Fluorescent Graphene Oxide Logic Gates for Discrimination of Iron (3+) and Iron (2+) in Living Cells by Imaging. *Chem. Commun.* **2012**, *48*, 7468−7470.

(9) Bastian, R.; Weberling, R.; Palilla, F. Determination of Iron by Ultraviolet Spectrophotometry. *Anal. Chem.* **1956**, *28*, 459−462.

(10) Talamond, P.; Doulbeau, S.; Rochette, I.; Guyot, J. P.; Treche, S. Anion-Exchange High-Performance Liquid Chromatography with Conductivity Detection for the Analysis of Phytic Acid in Food. *J. Chromatogr. A* **2000**, *871*, 7−12.

(11) Deprince, J.; Bautista, M.; Fritzsche, S.; García, J.; Kallman, T.; Mendoza, C.; Palmeri, P.; Quinet, P. K-Line X-Ray Fluorescence from Highly Charged Iron Ions under Dense Astrophysical Plasma Conditions. *X-Ray Spectrom.* **2020**, *49*, 29−32.

(12) Zhang, Y.; Xu, H.; Chen, Y.; You, X.; Pu, Y.; Xu, W.; Liao, X. High-Sensitivity Detection of Cysteine and Glutathione Using Au Nanoclusters Based on Aggregation-Induced Emission. *J. Fluoresc.* **2020**, *30*, 1491−1498.

(13) Lai, Q.; Liu, Q.; Zhao, K.; Duan, X.; Wang, G.; Su, X. Fluorometric Determination and Intracellular Imaging of Cysteine by Using Glutathione Capped Gold Nanoclusters and Cerium(III) Induced Aggregation. *Microchim. Acta* **2019**, *186*, 1−8.

(14) Ma, Y.; Abbate, V.; Hider, R. C. Iron-Sensitive Fluorescent Probes: Monitoring Intracellular Iron Pools. *Metallomics* **2015**, *7*, 212−222.

(15) Li, H.; Kang, Z.; Liu, Y.; Lee, S. T. Carbon Nanodots: Synthesis. Properties and Applications. *J. Mater. Chem.* **2012**, *22*, 24230−24253.

(16) Chung, S.; Revia, R. A.; Zhang, M. Graphene Quantum Dots and Their Applications in Bioimaging, Biosensing, and Therapy. *Adv. Mater.* **2021**, 1904362.
(17) Mai, X. D.; Thi Kim Chi, T.; Nguyen, T. C.; Ta, V. T. Scalable Synthesis of Highly Photoluminescence Carbon Quantum Dots. *Mater. Lett.* **2020**, *268*, 127595.
(18) Zhang, H.; Chen, Y.; Liang, M.; Xu, L.; Qi, S.; Chen, H.; Chen, X. Solid-Phase Synthesis of Highly Fluorescent Nitrogen-Doped Carbon Dots for Sensitive and Selective Probing Ferric Ions in Living Cells. *Anal. Chem.* **2014**, *86*, 9846−9852.
(19) Han, G.; Zhao, J.; Zhang, R.; Tian, X.; Liu, Z.; Wang, A.; Liu, R.; Liu, B.; Han, M. Y.; Gao, X.; et al. Membrane-Penetrating Carbon Quantum Dots for Imaging Nucleic Acid Structures in Live Organisms. *Angew. Chem., Int. Ed.* **2019**, *58*, 7087−7091.
(20) Ge, M.; Han, Y.; Ni, J.; Li, Y.; Han, S.; Li, S.; Yu, H.; Zhang, C.; Liu, S.; Li, J.; et al. Seeking Brightness from Nature: Sustainable Carbon Dots-Based AIEgens with Tunable Emission Wavelength from Natural Rosin. *Chem. Eng. J.* **2021**, *413*, 127457.
(21) Cao, L.; Wang, X.; Meziani, M. J.; Lu, F.; Wang, H.; Luo, P. G.; Lin, Y.; Harruff, B. A.; Veca, L. M.; Murray, D.; et al. Carbon Dots for Multiphoton Bioimaging. *J. Am. Chem. Soc.* **2007**, *129*, 11318−11319.
(22) Zhang, R.; Zhao, J.; Han, G.; Liu, Z.; Liu, C.; Zhang, C.; Liu, B.; Jiang, C.; Liu, R.; Zhao, T.; et al. Real-Time Discrimination and Versatile Profiling of Spontaneous Reactive Oxygen Species in Living Organisms with a Single Fluorescent Probe. *J. Am. Chem. Soc.* **2016**, *138*, 3769−3778.
(23) Zhang, Z.; Lei, Y.; Yang, X.; Shi, N.; Geng, L.; Wang, S.; Zhang, J.; Shi, S. High Drug-Loading System of Hollow Carbon Dots-Doxorubicin: Preparation,: In Vitro Release and PH-Targeted Research. *J. Mater. Chem. B* **2019**, *7*, 2130−2137.
(24) Wu, H.; Su, W.; Xu, H.; Zhang, Y.; Li, Y.; Li, X.; Fan, L. Applications of Carbon Dots on Tumour Theranostics. *View* **2021**, *2*, 20200061.
(25) Pal, A.; Sk, M. P.; Chattopadhyay, A. Recent Advances in Crystalline Carbon Dots for Superior Application Potential. *Mater. Adv.* **2020**, *1*, 525−553.
(26) Li, Y.; Xu, X.; Wu, Y.; Zhuang, J.; Zhang, X.; Zhang, H.; Lei, B.; Hu, C.; Liu, Y. A Review on the Effects of Carbon Dots in Plant Systems. *Mater. Chem. Front.* **2020**, *4*, 437−448.
(27) Miao, P.; Han, K.; Tang, Y.; Wang, B.; Lin, T.; Cheng, W. Recent Advances in Carbon Nanodots: Synthesis. Properties and Biomedical Applications. *Nanoscale* **2015**, *7*, 1586−1595.
(28) Wang, Q.; Liu, X.; Zhang, L.; Lv, Y. Microwave-Assisted Synthesis of Carbon Nanodots through an Eggshell Membrane and Their Fluorescent Application. *Analyst* **2012**, *137*, 5392−5397.
(29) Tian, X.; Murfin, L. C.; Wu, L.; Lewis, S. E.; James, T. D. Fluorescent Small Organic Probes for Biosensing. *Chem. Sci.* **2021**, *12*, 3406−3426.
(30) Liu, S.; Tian, J.; Wang, L.; Zhang, Y.; Qin, X.; Luo, Y.; Asiri, A. M.; Al-Youbi, A. O.; Sun, X. Hydrothermal Treatment of Grass: A Low-Cost, Green Route to Nitrogen-Doped, Carbon-Rich, Photoluminescent Polymer Nanodots as an Effective Fluorescent Sensing Platform for Label-Free Detection of Cu(II) Ions. *Adv. Mater.* **2012**, *24*, 2037−2041.
(31) Chen, Y.; Sun, X.; Pan, W.; Yu, G.; Wang, J. Fe3+-Sensitive Carbon Dots for Detection of Fe3+ in Aqueous Solution and Intracellular Imaging of Fe3+ Inside Fungal Cells. *Front. Chem.* **2020**, *7*, 1−9.
(32) Li, C.; Liu, W.; Ren, Y.; Sun, X.; Pan, W.; Wang, J. The Selectivity of the Carboxylate Groups Terminated Carbon Dots Switched by Buffer Solutions for the Detection of Multi-Metal Ions. *Sens. Actuators, B* **2017**, *240*, 941−948.
(33) Lu, S.; Sui, L.; Wu, M.; Zhu, S.; Yong, X.; Yang, B. Graphitic Nitrogen and High-Crystalline Triggered Strong Photoluminescence and Room-Temperature Ferromagnetism in Carbonized Polymer Dots. *Adv. Sci.* **2019**, *6*, 1801192.
(34) Ping, C. Determination of Serum Iron Content by Spectrophotometry. *Chinese J. Spectrosc. Lab.* **2012**, *29*, 1645−1648.
(35) Zhang, M.; Ju, H.; Zhang, L.; Sun, M.; Zhou, Z.; Dai, Z.; Zhang, L.; Gong, A.; Wu, C.; Du, F. Engineering Iodine-Doped Carbon Dots as Dual-Modal Probes for Fluorescence and X-Ray CT Imaging. *Int. J. Nanomed.* **2015**, *10*, 6943−6953.
(36) Jo, W. K.; Kumar, S.; Tonda, S. N-Doped C Dot/CoAl-Layered Double Hydroxide/g-C3N4 Hybrid Composites for Efficient and Selective Solar-Driven Conversion of CO2 into CH4. *Compos. Part B Eng.* **2019**, *176*, 107212.
(37) Cunha, E.; Proença, M. F.; Pereira, M. G.; Fernandes, M. J.; Young, R. J.; Strutyński, K.; Melle-Franco, M.; Gonzalez-Debs, M.; Lopes, P. E.; Da Conceição Paiva, M. Water Dispersible Few-Layer Graphene Stabilized by a Novel Pyrene Derivative AtMicromolar Concentration. *Nanomaterials* **2018**, *8*, 1−17.
(38) Varsha Sasikumar, S. P.; Palanichamy, K.; Sasirekha, N. R.; Rajashree, P. Facile Preparation of Carbon Dots from Chrysanthemum Morifolium. *AIP Conf. Proc.* **2019**, *2115*, 1−15.
(39) Bhamore, J. R.; Park, T. J.; Kailasa, S. K. Glutathione-Capped Syzygium Cumini Carbon Dot-Amalgamated Agarose Hydrogel Film for Naked-Eye Detection of Heavy Metal Ions. *J. Anal. Sci. Technol.* **2020**, *11*, 1−9.
(40) Zhang, Y.; Khan, M. Z. H.; Yuan, T.; Zhang, Y.; Liu, X.; Du, Z.; Zhao, Y. Preparation and Characterization of D. Opposita Thunb Polysaccharide-Zinc Inclusion Complex and Evaluation of Anti-Diabetic Activities. *Int. J. Biol. Macromol.* **2019**, *121*, 1029−1036.
(41) Liu, Z.; Zu, Y.; Fu, Y.; Meng, R.; Guo, S.; Xing, Z.; Tan, S. Hydrothermal Synthesis of Histidine-Functionalized Single-Crystalline Gold Nanoparticles and Their PH-Dependent UV Absorption Characteristic. *Colloids Surfaces B Biointerfaces* **2010**, *76*, 311−316.
(42) Bano, D.; Chandra, S.; Yadav, P. K.; Singh, V. K.; Hasan, S. H. Off-on Detection of Glutathione Based on the Nitrogen, Sulfur Codoped Carbon Quantum Dots@MnO2 Nano-Composite in Human Lung Cancer Cells and Blood Serum. *J. Photochem. Photobiol., A* **2020**, *398*, 112558.
(43) Zhou, J.; Wang, C.; Qian, Z.; Chen, C.; Ma, J.; Du, G.; Chen, J.; Feng, H. Highly Efficient Fluorescent Multi-Walled Carbon Nanotubes Functionalized with Diamines and Amides. *J. Mater. Chem.* **2012**, *22*, 11912−11914.
(44) Bhattacharyya, A.; Schmidt, M. P.; Stavitski, E.; Martínez, C. E. Iron Speciation in Peats: Chemical and Spectroscopic Evidence for the Co-Occurrence of Ferric and Ferrous Iron in Organic Complexes and Mineral Precipitates. *Org. Geochem.* **2018**, *115*, 124−137.
(45) Meyer-Almes, F. J. Fluorescence Lifetime Based Bioassays. *Methods Appl. Fluoresc.* **2017**, *5*, No. 042002.
(46) Wang, X.; Qu, K.; Xu, B.; Ren, J.; Qu, X. Microwave Assisted One-Step Green Synthesis of Cell-Permeable Multicolor Photoluminescent Carbon Dots without Surface Passivation Reagents. *J. Mater. Chem.* **2011**, *21*, 2445−2450.
(47) Dhenadhayalan, N.; Lin, K. C. Chemically Induced Fluorescence Switching of Carbon-Dots and Its Multiple Logic Gate Implementation. *Sci. Rep.* **2015**, *2015*, 10012.
(48) Wu, K. Y.; Qin, L.; Fan, C.; Cai, S. L.; Zhang, T. T.; Chen, W. H.; Tang, X. Y.; Chen, J. X. Sequential and Recyclable Sensing of Fe3+ and Ascorbic Acid in Water with a Terbium(Iii)-Based Metal-Organic Framework. *Dalt. Trans.* **2019**, *48*, 8911−8919.
(49) Shamsipur, M.; Molaei, K.; Molaabasi, F.; Alipour, M.; Alizadeh, N.; Hosseinkhani, S.; Hosseini, M. Facile Preparation and Characterization of New Green Emitting Carbon Dots for Sensitive and Selective off/on Detection of Fe3+ Ion and Ascorbic Acid in Water and Urine Samples and Intracellular Imaging in Living Cells. *Talanta* **2018**, *183*, 122−130.
(50) Yi, D.; Wu, Y.; Chen, C.; Wang, L.; Wang, Q.; Pu, L.; Wei, S. Preparation of Pyrido[1,2-c][1,2,4]Triazole-Based π-Conjugated Triazene as a Fe 3+ Ion Fluorescent Sensor. *Chinese Chem. Lett.* **2019**, *30*, 1059−1062.
(51) Wang, Q.; Berglund, K. A. Pyranine Fluorescence Quenching for the Characterization of Solutions. *Am. J. Anal. Chem.* **2016**, *07*, 43−56.
(52) Perosa, A.; Selva, M.; Lucchini, V.; Fabris, M.; Noè, M. Kinetic Parameter Estimation of Solvent-Free Reactions Monitored by 13C NMR Spectroscopy, a Case Study: Mono- and Di-(Hydroxy)-

https://doi.org/10.1021/acsomega.1c06757
ACS Omega 2022, 7, 7853−7864

Ethylation of Aniline with Ethylene Carbonate. *Int. J. Chem. Kinet.* **2011**, *43*, 154−160.

https://doi.org/10.1021/acsomega.1c06757
ACS Omega 2022, 7, 7853−7864